

# Identification of High $p_{\perp}$ Particles with the STAR-RICH Detector

The STAR-RICH Collaboration: A. Braem<sup>a</sup>, D. Cozza<sup>b</sup>,  
M. Davenport<sup>a</sup>, G. De Cataldo<sup>b</sup>, L. Dell Olio<sup>b</sup>, D. DiBari<sup>b</sup>,  
A. DiMauro<sup>a</sup>, J. C. Dunlop<sup>c</sup>, E. Finch<sup>d</sup>, D. Fraissard<sup>a</sup>, A. Franco<sup>b</sup>,  
J. Gans<sup>c</sup>, B. Ghidini<sup>b</sup>, J. W. Harris<sup>c</sup>, M. Horsley<sup>c</sup>, G. J. Kunde<sup>c</sup>,  
B. Lasiuk<sup>c</sup>, Y. Lesenechal<sup>a</sup>, R. D. Majka<sup>d</sup>, P. Martinengo<sup>a</sup>,  
A. Morsch<sup>a</sup>, E. Nappi<sup>b</sup>, G. Paic<sup>a</sup>, F. Piuz<sup>a</sup>, F. Posa<sup>b</sup>, J. Raynaud<sup>a</sup>,  
S. Salur<sup>c</sup>, J. Sandweiss<sup>d</sup>, J. C. Santiard<sup>a</sup>, J. Satinover<sup>c</sup>, E. Schyns<sup>a</sup>,  
N. Smirnov<sup>c</sup>, J. Van Beelen<sup>a</sup>, T. D. Williams<sup>a</sup>, Z. Xu<sup>d</sup>

<sup>a</sup>CERN HMPID group, CERN, Geneva CH-1211

<sup>b</sup>Bari HMPID Group, Bari, Sez. INFN and Dipartimento di fisica, 70124, Italy

<sup>c</sup>Yale RHI Group, New Haven, CT 06520-8124, USA

<sup>d</sup>Yale HE Group, New Haven, CT 06520, USA

---

## Abstract

The STAR-RICH detector extends the particle identification capabilities of the STAR experiment for charged hadrons at mid-rapidity. This detector represents the first use of a proximity-focusing CsI-based RICH detector in a collider experiment. It provides identification of pions and kaons up to 3 GeV/c and protons up to 5 GeV/c. The characteristics and performance of the device in the inaugural RHIC run are described.

---

## 1 Introduction

Penetrating probes are of importance for the study of the dense partonic matter formed after the collision of heavy nuclei at RHIC energies. At RHIC a new regime is reached, in which the collisions are semihard, producing so-called minijets. In nucleon-nucleon collisions the behavior of minijets and the spectra of the particles emitted in minijets are amenable to perturbative

QCD calculations, and thus represent a firm ground for comparison with experiments. In nucleus-nucleus collisions particles produced in the initial state of the collision (before thermalization) are used to “probe” the matter formed in the collision. By measuring the momentum spectra of identified particles a picture characteristic of the matter they have traversed will be obtained [1]. This makes, among other probes, the measurement of identified

particles at high momentum an essential objective of heavy-ion detectors.

To achieve this goal the STAR detector has complemented its particle identification at low momenta (achieved with the TPC and SVT until 0.6 and 1 GeV/c, for kaons and protons, respectively) with a patch of detector dedicated to high momentum identification, based on the identification of photon patterns emitted by Cherenkov radiation.

The STAR-RICH proximity-focusing Ring Imaging Cherenkov (RICH) detector was originally built as a 1 m<sup>2</sup> prototype for the HMPID (High Momentum Particle Identification) detector of the ALICE experiment at the LHC [2]. After extensive and fully satisfactory tests at the H4 line of the CERN SPS it was decided to install it in STAR [3]. The STAR-RICH detector covers 2% of the TPC acceptance and has been installed in the central rapidity region covering  $\Delta\eta < 0.3$ , for event vertices at the center of the TPC, and  $\Delta\phi = 20^\circ$ . Using this detector, the momentum range of particle identification should be extended to 3 GeV/c for kaons and 5 GeV/c for protons. The present detector represents the first use of a proximity-focusing RICH detector, with a MWPC pad cathode coated with CsI, in a collider experiment. In the following we will describe the detector and its performance. In the last part we will present the pattern recognition algorithm applied to the data.

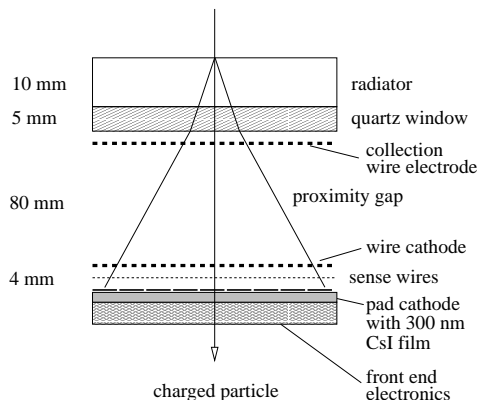


Fig. 1. Cutaway view of the detector[2].

## 2 Characteristics

A schematic of the detector is shown in figure 1. The Cherenkov photon radiating medium is a 1 cm thick layer of liquid perfluorohexane ( $C_6F_{14}$ ) circulated into a tray, closed by a 0.5 cm thick UV-grade fused silica plate in order to match the spectral range of the photoconverter. Two such trays of 1330x413 mm<sup>2</sup> size are implemented in this detector.

Using a proximity RICH geometry, the distance radiator to photodetector is fixed at 80 mm for optimization of pattern recognition [4]. Electrons released by ionizing particles in the proximity gap are prevented from entering the photodetector volume by a positive polarization of the collection electrode close to the radiator.

The photodetector is made of a conventional MWPC having one of the cathode plane segmented into pads of 8.0x8.4 mm<sup>2</sup> area at a distance of 2 mm from the anode plane, which consists of 20  $\mu\text{m}$  diameter wires spaced by 4.2 mm. The opposite cathode consists of 100  $\mu\text{m}$  wires, spaced by 2.1 mm

and located at 2.2 mm from the anode plane. Four independent panels, of  $640 \times 400 \text{ mm}^2$  sensitive area, form the cathode plane, resulting in a total active area of  $1280 \times 800 \text{ mm}^2$ .

The photoconverter consists of a thin layer of CsI deposited under vacuum on the pad cathode surface. The useful spectral range of such a photocathode is limited between the CsI threshold at 205 nm and the radiator transparency at 170 nm. It has been demonstrated that such a photocathode can be operated under gas at atmospheric pressure with a yield of  $17 \pm 2$  reconstructed photoelectron clusters per ring for  $\beta \sim 1$ , at a gas gain of  $0.8 - 2. \times 10^5$  [2,4,5,6]. If kept under inert gas flow, the photocathode has a quantum efficiency stable over several years. It can be operated in an “open MWPC geometry” without suffering from photon feedback. An accurate localization of the particles can be achieved by charge centroid calculation with this photocathode.

The electronics readout is implemented at the back of the pad panels. Given the modest event rate expected around ion colliders, it is based on the ASIC GASSIPLEX chip providing 16 analog multiplexed channels [7]. In the STAR-RICH application 60 chips (960 channels) are daisy chained in order to minimize the number of expensive ADCs while keeping the readout time compatible with the RHIC interaction rate. The digitization and zero-suppression are performed by using the commercial CAEN V550 ADC VME module. The multiplexing frequency is 1 MHz and the noise level on the detector is of the order of 1000 e- r.m.s over 15360

channels in total.

A detailed description of these elements and of the beam test measurements performed can be found in references [2,4,5,6,8].

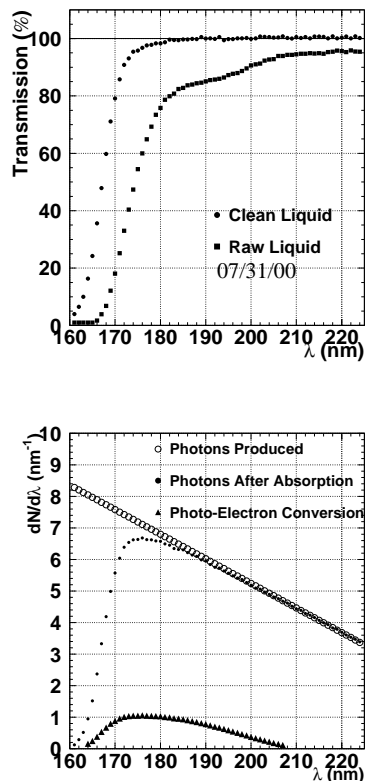


Fig. 2. Top: the measured transmission of the liquid radiator in raw (squares) and cleaned (circles) form. Bottom: the simulated spectrum of Cherenkov light produced in the liquid radiator (open circles) and the effect of the finite liquid and quartz transmission. The resulting spectrum transmitted to the pad plane (solid circles) is folded with the quantum efficiency of the CsI to show the spectrum of photons converted to electrons (triangles).

CsI has a photo-electric threshold of 205 nm (6.0 eV) which restricts its sensitivity to vacuum ultra-violet (VUV) photons. This imposes constraints on the spectral properties of the radiator

medium, its containment vessel, as well as the MWPC gas. In order to extend the PID capabilities of the TPC, a radiator with an index of refraction in the range of 1.2-1.3 is necessary. Perfluorohexane ( $C_6F_{14}$ ) has an index of refraction of 1.3 at 170 nm [8], and shows transparency to VUV radiation down to 152 nm, if water and oxygen are reduced to the ppm level. Pure methane is utilized as the MWPC gas since it is transparent to VUV radiation down to 130 nm and allows the chamber to be run in a stable manner at a gas gain of  $\sim 10^5$  with no deterioration of quantum efficiency up to a rate density of  $2.0 \times 10^4 s^{-1} cm^{-1}$  [6]. The importance of a transparent radiator medium is depicted in figure 2. The top panel shows the measured transmission of the liquid before and after cleaning while the bottom panel shows the simulated spectrum of Cherenkov light incident on the pad plane and subsequently converted to photo-electrons.

In addition to the spectral constraints CsI imposes, it is also hygroscopic and care must be taken to isolate it from water, as well as oxygen. From experience accumulated over the past 5 years and six large CsI photocathodes, the following observations can be reported. Keeping the CsI photocathode under permanent flow of Argon (10-15 l/h) in a protective sealed metallic enclosure of volume 1.5 l with moisture levels of less than 20 ppm resulted in a reduction of less than 10% in quantum efficiency over 5 years. Exposing a CsI photocathode to 200 ppm moisture for 30 hours without argon flow and to  $1.10 \times 10^5$  ppm oxygen for 20 hours had no effect on the quantum efficiency, following tests done at CERN

test beams with the quantum efficiency measured before and after exposure to contaminants. This last point was a significant consideration in transporting the detector from CERN to BNL, providing constraints on the construction of a sealed transportation vessel [9].

### 3 Performance and Analysis

The STAR-RICH capability to identify charged particles has been studied in central Au+Au collisions ( $\sqrt{s_{NN}} = 130$  GeV) during the first year of running of RHIC, where about 900k central and 900k minimum bias triggers have been recorded. The identification of high momentum charged particles in STAR ( $p > 1$  GeV/c) can be performed once the momentum and the velocity,  $\beta$ , for each particle, are measured. The STAR-RICH detector allows for measurement of the  $\beta$  of the particle by the reconstruction of the Cherenkov angle, while the momentum of the track is obtained from the TPC.

Extrapolation of tracks to the RICH show a distribution of residuals, between the projected impact point of the track and the centroid of a cluster with charge  $Q > 120$  ADC (see figure 3), with a  $\sigma$  of 4 mm for tracks with a momentum greater than 1 GeV/c. Tracks with smaller momentum have a much larger width since multiple scattering becomes more appreciable. Tracks with residuals  $< 5$  mm are selected for further analysis. This requirement mainly rejects those particles that, although reconstructed in the TPC, are not detected in the STAR-RICH detector because they either undergo an

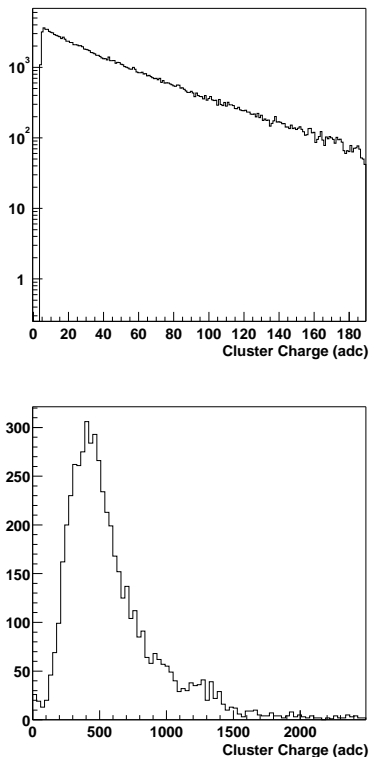


Fig. 3. Charge spectrum of reconstructed clusters in the chamber. Top: hits within the expected fiducial area for photons. Bottom: hits within 0.5 cm of a projected TPC track. Overflows affect the spectrum above  $\sim 950$  ADC counts.

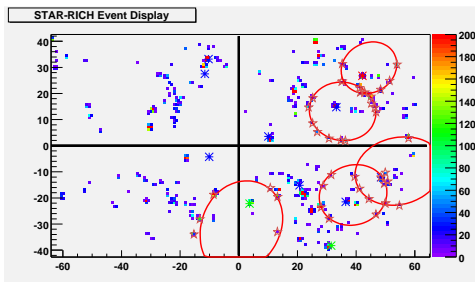


Fig. 4. An off-line event display of the RICH detector. Colored squares show the ADC value for pads with charge above threshold. Reconstructed rings are shown for associated tracks.

upstream interaction with the material between the TPC and the STAR-RICH or decay.

After having selected a track candi-

date, an algorithm for the recognition of Cherenkov patterns based on the Hough transform method is applied. It consists of a mapping of the pad coordinate space directly to the parameter space of the Cherenkov photon angle, extracted from the photon cluster coordinate by a geometrical back-tracking. More details can be found in reference [10]. This method is efficient even in the presence of large occupancy. In central collisions in STAR, however, the pad occupancy never exceeds 5%, corresponding to a good Cherenkov photon signal to noise ratio. The pattern generated by the detected photoelectrons is a function of the track incident angle. A mean value of about  $7^\circ$  is obtained for tracks with  $|\eta| < 0.15$  coming from a primary vertex with  $|\text{vertex } z| < 50$  cm. This produces Cherenkov patterns with elliptical shapes. Figure 4 shows the offline display of an event in the RICH detector, where the reconstructed rings associated to tracks with momentum  $> 1$  GeV/c have been also drawn.

The reconstructed Cherenkov angle as a function of the track momentum is shown in figure 5. Bands with low background, centered around the predicted curves for pions, kaons, and protons, can clearly be seen. Figure 6 shows an example of the distribution of the reconstructed Cherenkov angle, in a small interval of transverse momentum, where the three peaks corresponding to pions, kaons, and protons are clearly visible. This distribution is fitted in order to extract the relative yields.

In an alternative method, three mass hypotheses are made for a given track

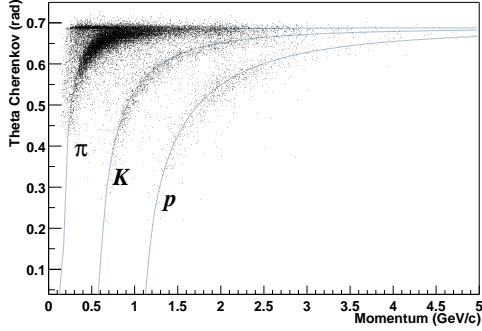


Fig. 5. Reconstructed Cherenkov angle in the RICH vs momentum from the TPC.

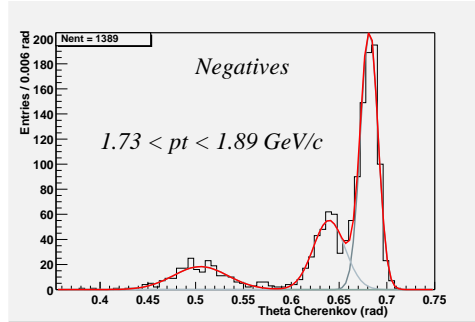


Fig. 6. Reconstructed Cherenkov angle in the RICH in a restricted range of transverse momentum measured by the TPC.

( $\pi$ ,  $K$ , and  $p$ ). The limiting bounds of the Cherenkov rings, defined by the dimensions of the radiator vessel, are projected on to the pad plane. The mass of the particle can be assigned by selecting the band with the highest density of photons, from which yields can be extracted.

## 4 Conclusion

A proximity-focusing CsI RICH detector, developed by the ALICE collaboration, has been installed in the STAR detector at RHIC, representing the first use of such a device in a collider experiment. This device extends the PID capabilities of the spectrometer to 3 GeV/c for pions and kaons, and

5 GeV/c for protons. The performance of the detector is within expectations, which will allow an examination of the effect of matter at high density on high  $p_{\perp}$  particles in the coming years.

## References

- [1] For example, see X. N Wang, Phys. Rev **C58** (1998) 2231.
- [2] F. Piuz et al, NIM **A433** (1999) 178-189.
- [3] STAR-RICH collaboration, *Proposal for a Ring Imaging Cherenkov Detector in STAR*, YRHI 98-022.
- [4] A. Di Mauro et al, NIM **A433** (1999) 190-200.
- [5] F. Piuz et al, NIM **A433** (1999) 222-234.
- [6] A. Di Mauro et al, NIM **A371** (1996) 137.
- [7] J.C. Santiard et al, *GASSIPLEX, a low noise analog signal processor for readout of gaseous detectors*, CERN-ECP 94-17.
- [8] ALICE collaboration, *ALICE Technical Design Report: Detector for High Momentum PID*, CERN/LHCC 98-19.
- [9] A. Di Mauro et al., NIM **A461** (2001) 584.
- [10] D. Elia et al., NIM. nnnn**A433** (1999) 262.